SI Appendix for "Plastic debris in the open ocean"

Authors: Andrés Cózar, Fidel Echevarría, Juan I. González-Gordillo, Xabier Irigoien, Bárbara Úbeda, Santiago Hernández-León, Álvaro T. Palma, Sandra Navarro, Juan García-de-Lomas, Andrea Ruiz, María L. Fernández-de-Puelles, Carlos M. Duarte.

Files in this SI Appendix:

Tables S1 to S2
Figures S1 to S13
References S1 to S17

Table S1. Sampling details by source. "Wind-corrected grid cells" indicates the number of 2º x 2º averaged data included in the wind-corrected dataset. "Non-corrected grid cells" indicates the number of 2º x 2º averaged data used for the low estimate of surface plastic pollution. This dataset included data reported by other authors and classified as affected by high wind conditions. Spatial distribution of data by source is shown in Fig. S1. The number of tows by ocean is shown in Table S2.

Region	Wind-corrected grid cells	Non-corrected grid cells	Period	Original unit	Mesh size	Source (vessel)
Malaspina Circumnavigation	141	141	December 2010 to July 2011	g km^{-2}	200 μm	this study (RV Hesperides)
northeastern North Atlantic	12	12	June 2011 to September 2011	g km^{-2}	200 μm	this study (RV Pakea)
southeastern South Atlantic	9	9	December 2012 to February 2013	g km^{-2}	200 μm	this study (RV Pakea)
eastern South Pacific	3	3	March 2009 to November 2011	g km^{-2}	200 μm	this study (RV Poli)
central South Pacific	6	6	March 2012	g km^{-2}	200 μm	this study (RV Aquiles)
west-to-east transect across the North Atlantic	14	14	March 2011	g km^{-2}	1000 μm	this study (RV Sarmiento)
eastern North Atlantic	48	112	February 2006 to December 2008	items km^{-2}	335 μm	ref. (S1)
California Current System (eastern North Pacific)	14	14	April 2006 to January 2007	mg m^{-3}	505 μm	ref. (S2)
Bering Sea (northeastern North Pacific)	3	8	May 2006 to September 2006	mg $m^{-3)}$	505 μm	ref. (S2)
off Vancouver Island (northeastern North Pacific)	2	6	April 2006	mg m^{-3}	505 μm	ref. (S2)
Tropical Pacific	2	9	August 2006 to October 2006	mg m^{-3}	505 μm	ref. (S3)
eastern North Pacific	24	42	August 2009 to October 2010	mg m^{-3}	333 μm	ref. (S3)
east-to-west transect across central South Pacific	15	26	March 2011 to April 2011	g km^{-2}	333 μm	ref. (S4)
waters around Australia	51	51	June 2011 to August 2012	items km^{-2}	333 μm	ref. (S5)
eastern Pacific Ocean	98	398	February 2006 to December 2012	Items km^{-2}	333 μm	ref. (S6)

Table S2. Number of sampled grid cells and surface net tows by oceans for the two datasets used in the spatial analysis of plastic pollution.

	Wind-corrected dataset		Non-corrected dataset	
	Grid cells	**Net tows**	**Grid cells**	**Net tows**
North Atlantic Ocean	106	233	170	658
North Pacific Ocean	175	548	440	1682
South Atlantic Ocean	37	54	37	54
South Pacific Ocean	72	165	152	549
Indian Ocean	52	127	52	127
Global Ocean	442	1127	851	3070

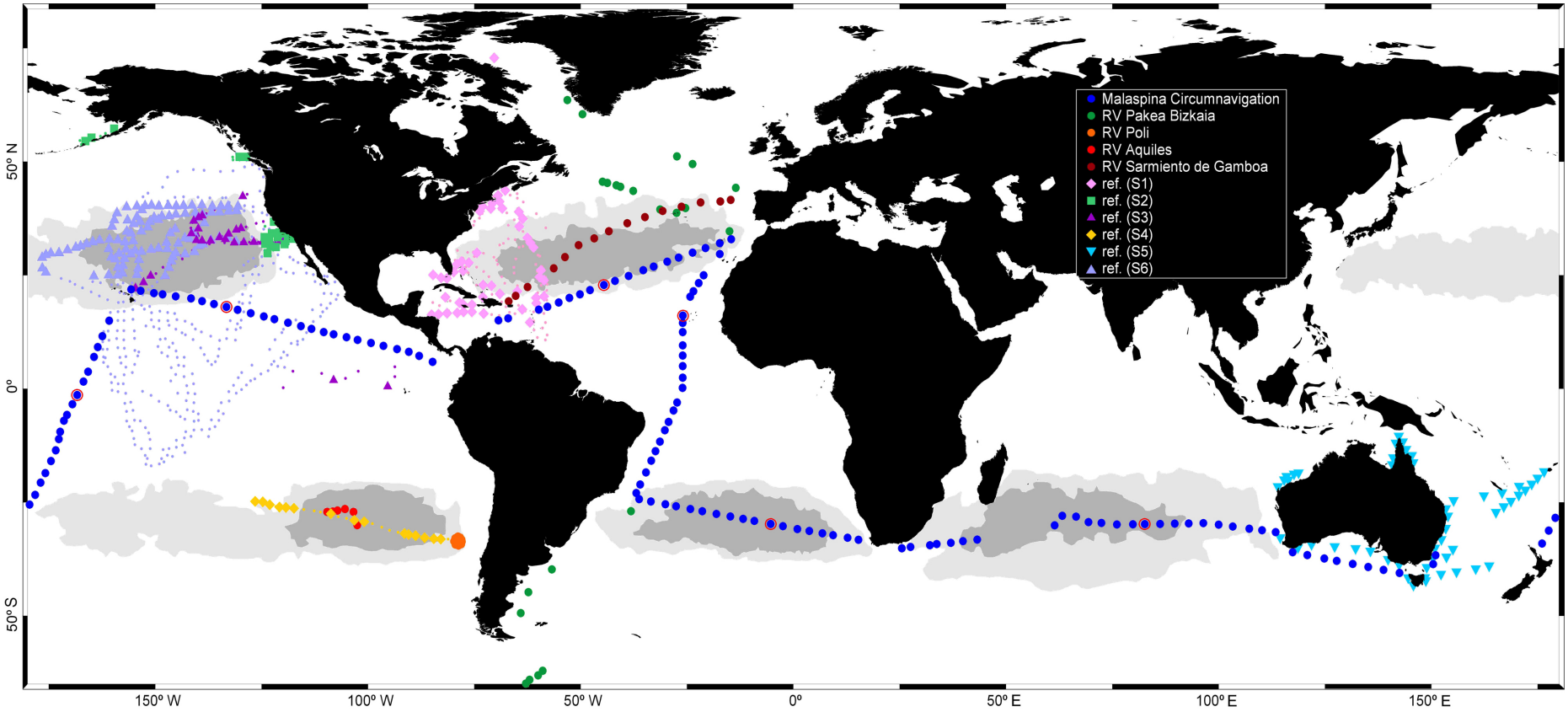

Fig. S1. Spatial distribution of data by sources. Figure legend indicates the vessel for the original data and the bibliographic reference for the datasets published. Large solid symbols show wind-corrected data (442 grid cells, 1127 surface net tows). Small dots show literature data classified as affected by high wind conditions and not included in the wind-corrected dataset (409 grid cells, 1943 surface net tows). Sampling sites where size distribution of non-plastic particles was measured are marked with red circles (see Fig. S12).

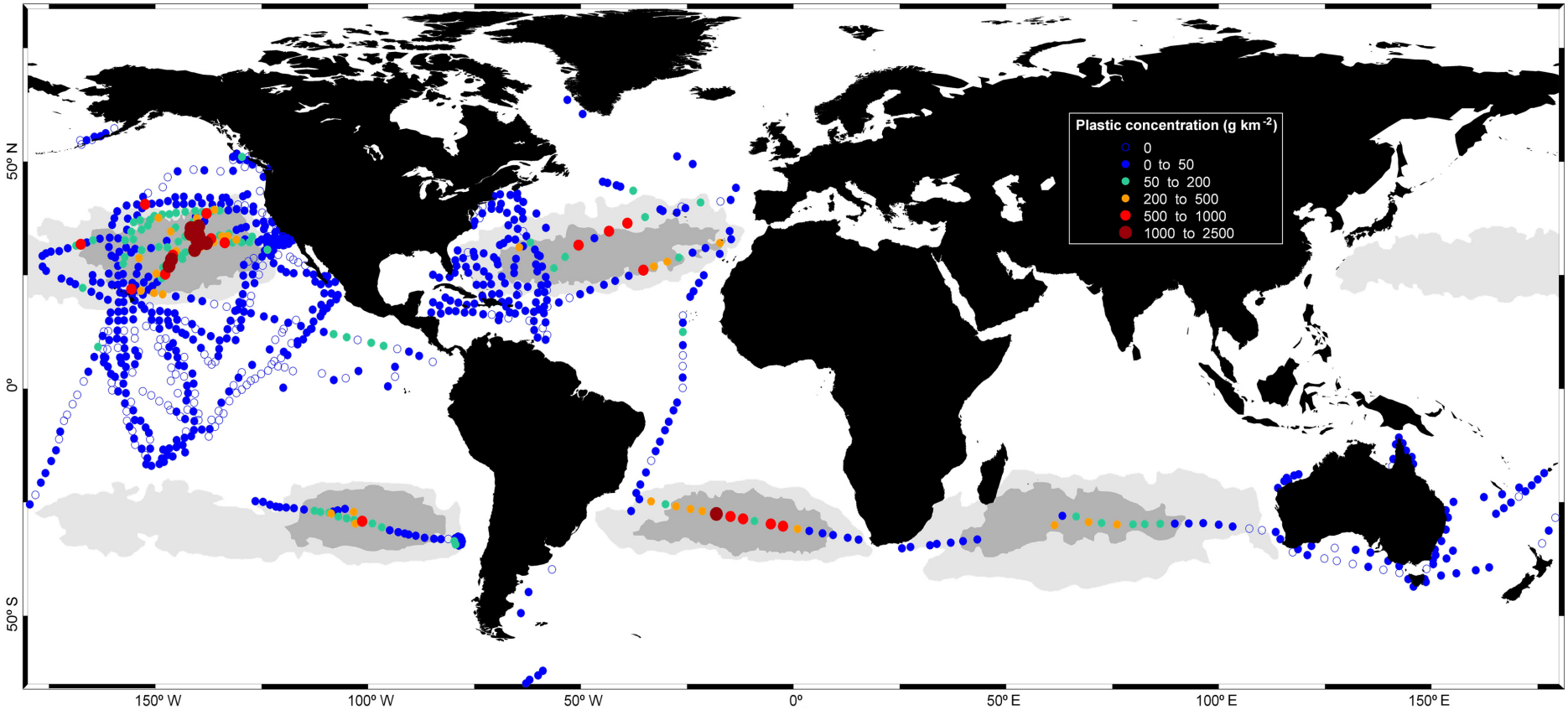

Fig. S2. Measurements of plastic concentrations without correction by wind conditions (non-corrected dataset). Color circles indicate mass concentrations (legend on top right). The dataset includes average concentrations in 851 sites (3070 surface net tows). Low estimate of plastic load was derived from this dataset.

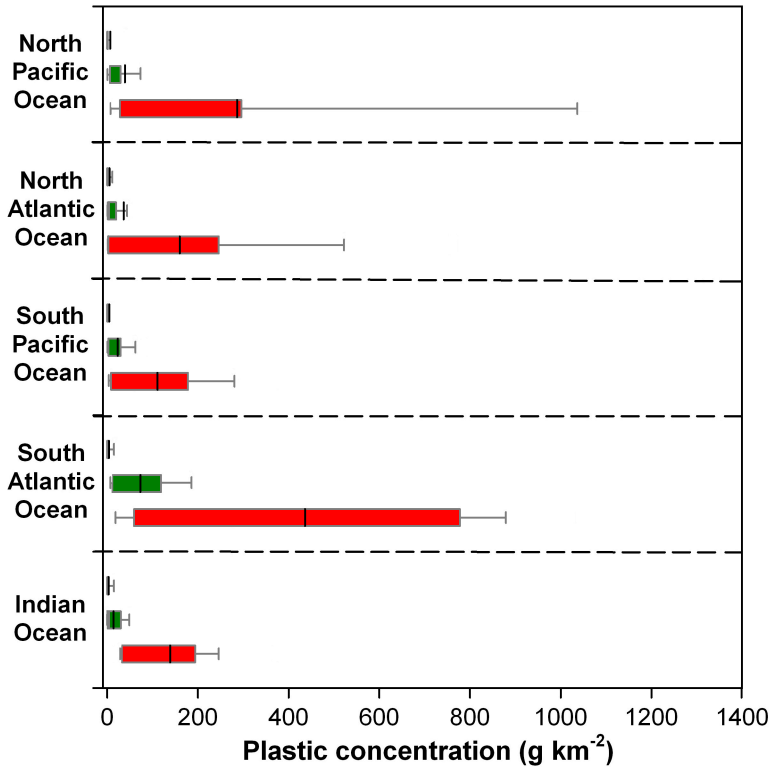

Fig. S3. Ranges of surface plastic concentrations calculated from the non-corrected database. Non-accumulation zone (blue boxes), outer accumulation zone (green boxes) and inner accumulation zone (red boxes). The boundaries of the boxes indicate the 25th and 75th percentiles, the black lines within the box mark the mean, and the whiskers above and below the boxes indicate the 90^{th} and 10^{th} percentiles. Data used for this graph are mapped in Fig. S2.

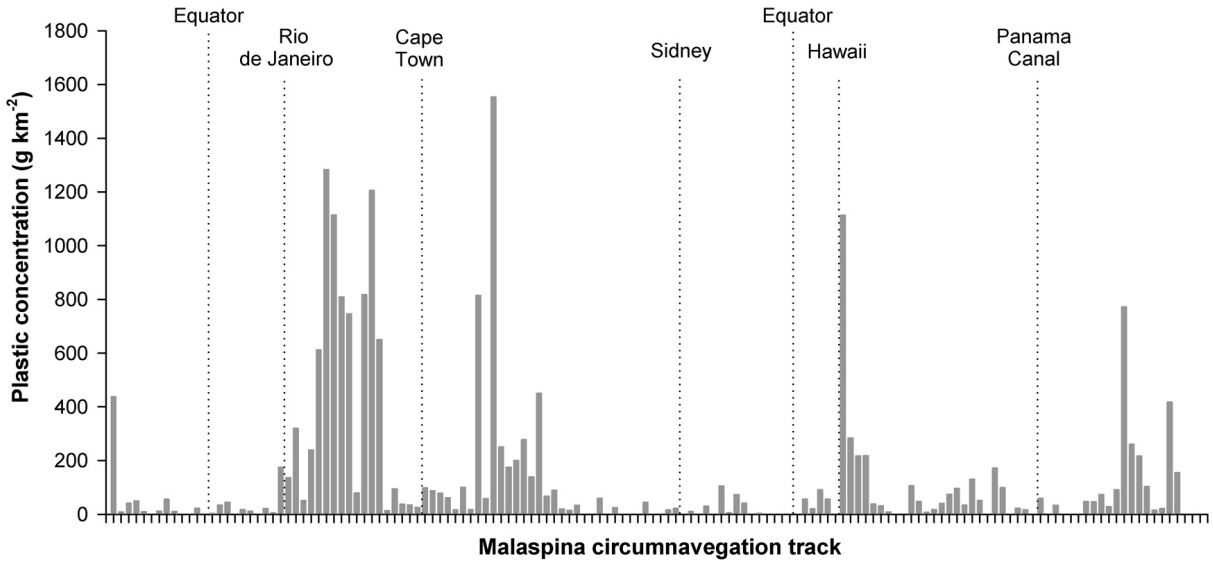

Fig. S4. Plastic concentrations along the Malaspina Circumnavigation from Cadiz to Cadiz (Spain). Every sampling site (blue circles in Fig. S1) is marked with a tick in the horizontal axis.

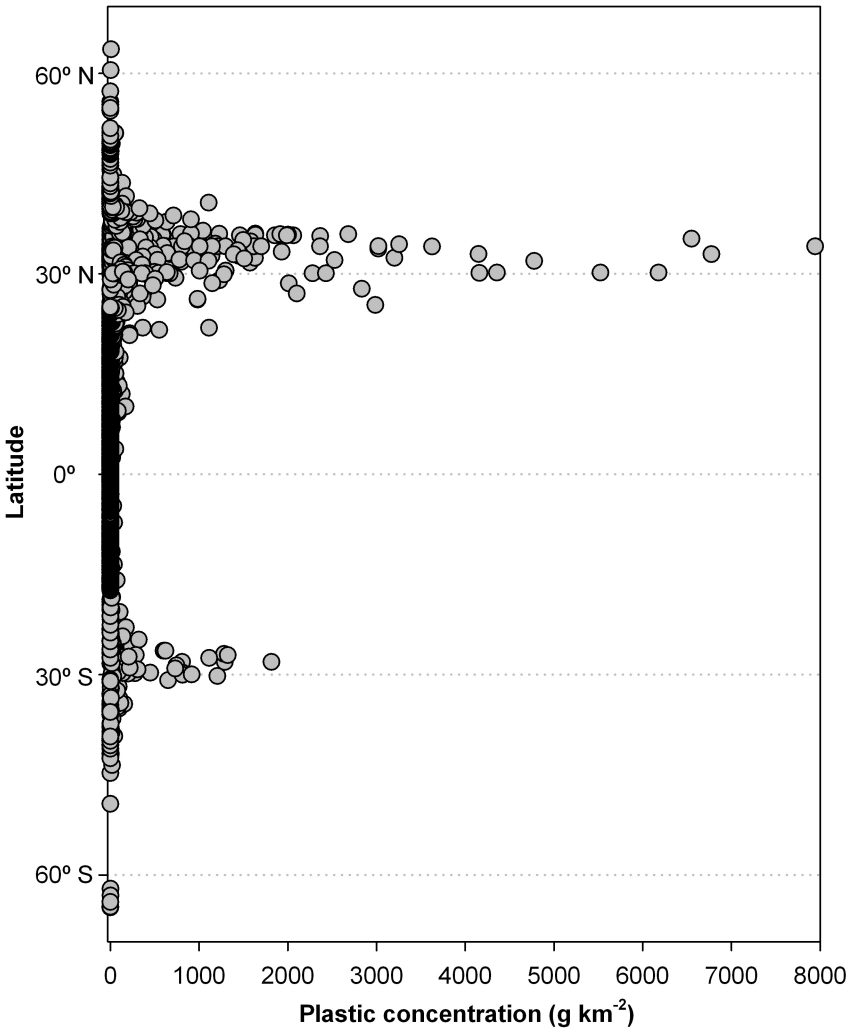

Fig. S5. Plastic concentrations as a function of latitude.

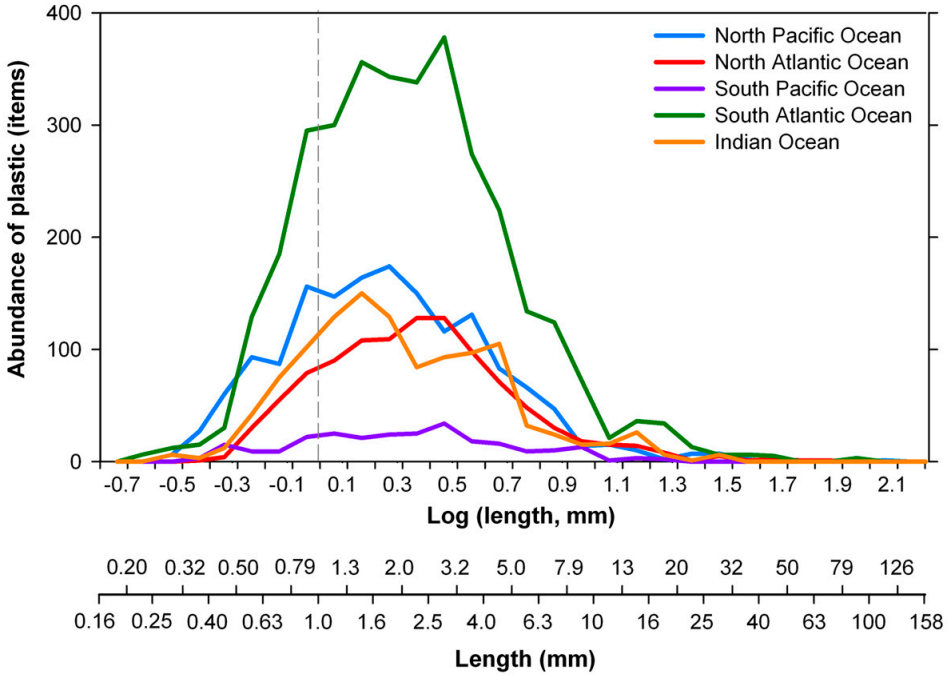

Fig. S6. Size distributions of plastic fragments by ocean basin. Size distributions were built with the plastic items collected along the circumnavigation: 1565 in North Pacific Ocean, 1043 items in North Atlantic Ocean, 259 items in South Pacific Ocean, 3339 items in South Atlantic Ocean, and 1153 items in Indian Ocean. The gap in the plastic size distributions below 1 mm was present in all ocean basins. Dashed vertical line corresponds to 1 mm size limits.

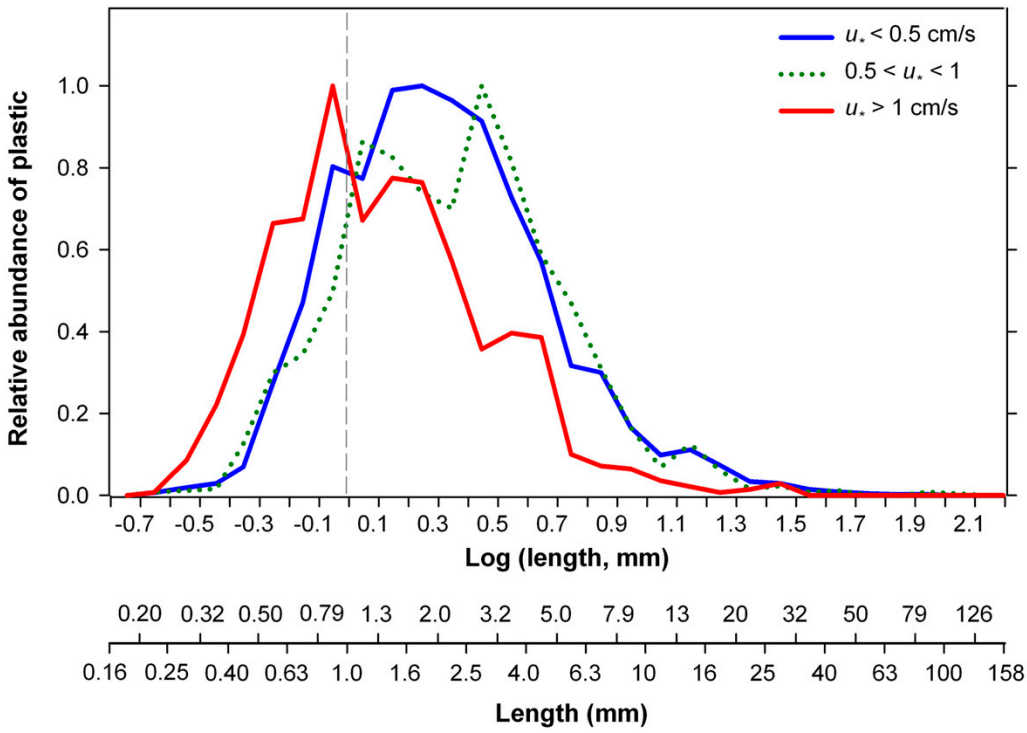

Fig. S7. Size distributions of surface plastic fragments for different wind conditions. Wind categories were established according to the u_* thresholds at which the effect of wind mixing on surface plastic abundance are predicted to be low (< 0.5 cm/s; 4184 plastic items), moderate (0.5 – 1 cm/s, 2138 items) and high (> 1 cm/s, 1037 items) (S7). For comparative purposes, these size distributions are shown as abundance in relation to the maximal abundance in the size classes. The comparison of confidence intervals of the means by inferential statistic only showed significant differences between the size distribution at high wind stress (> 1 cm/s) and the other two size distributions (< 0.5 cm/s and 0.5 – 1 cm/s). We found higher relative abundance of small particles (< 1 mm) in tows with high wind stress. The surface abundance of particles must decrease with wind stress due to vertical turbulent diffusion of buoyant particles throughout the surface wind-mixed layer. However, turbulence also leads to a size-selective increase of the vertical velocity resulting from the positive buoyancy of the particles (S8, S9). Theoretical considerations and empirical results evidence that upward velocities of particles sized around the Kolmogorov micro-scale (λ, the smallest length scale of the turbulence eddies) are very sensitive to turbulence levels. Their upward velocity may increase by two orders of magnitude more than those larger or smaller than λ (S9). Given that λ ranges from 0.3 to 2 mm for the wind-driven oceanic turbulence (S10), this process could explain the preferential accumulation of particles in the lower part of our size spectrum at high wind stress since they are around the same size as λ. These results allow us to conclude that the gap below 1 mm is not related to the wind effect.

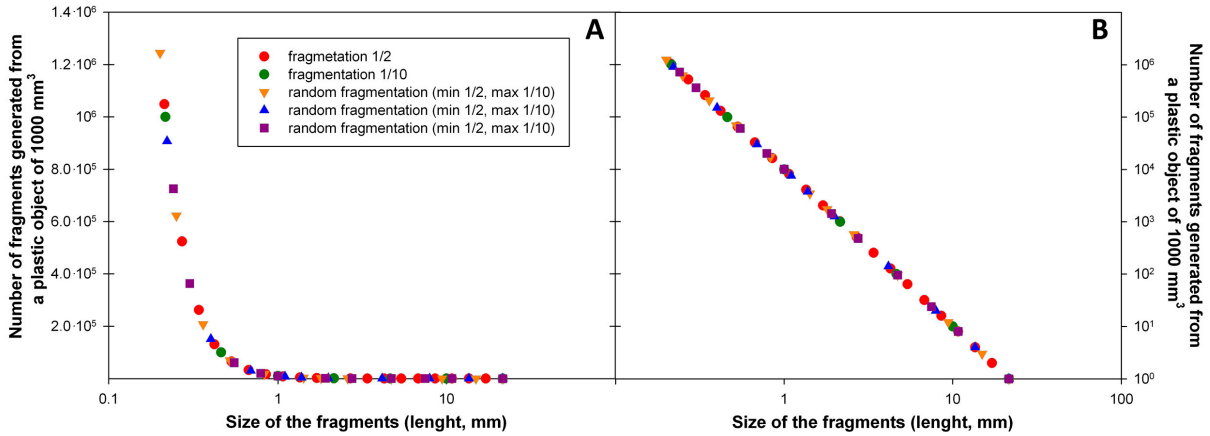

Fig. S8. Number of fragments generated from a plastic object of 1000 mm^3 using different fragmentation modes (see legend in A). Y-axis is lineal in A, and logarithmic in B. The length of the pieces was computed as $(volume/\alpha)^{1/3}$, being $\alpha = 0.1$. A plastic object successively broken down into half (fragmentation 1/2) would generate 2^n pieces, with n being the number of times broken down. And a plastic object successively broken down into ten pieces (fragmentation 1/10) would generate 10^n pieces. Note that the number of fragments of a specific size that a plastic object may generate depends on the original volume of the object, but it is independent of the number of pieces generated in each fragmentation event (e.g. 1/2 or 1/10) or the number of fragmentation events required (n). The exponent of the power law relationship described by the simulations is 3, regardless of the α value (shape of the object) used in the simulation. Therefore, a stable input and fragmentation of large plastic objects should lead to a power-law size distribution with a scaling exponent of 3. The exponent of the power-law part in the observed size distribution (size range: 5-100 mm, 14 size classes) confirmed this prediction (2.93 ±0.08 at calm conditions, Fig. 3; 2.98 ±0.13 using all tows in the circumnavigation, Fig. S10). This finding suggests that the fragmentation progressively proceeds in the three spatial dimensions of the objects (length, width and height), as observed in experiments of accelerated aging of plastic material (S11). Accordingly, the abundance-size distribution derived from fragmentation would depend on the large-plastic volume entering the ocean, being independent of plastic shape.

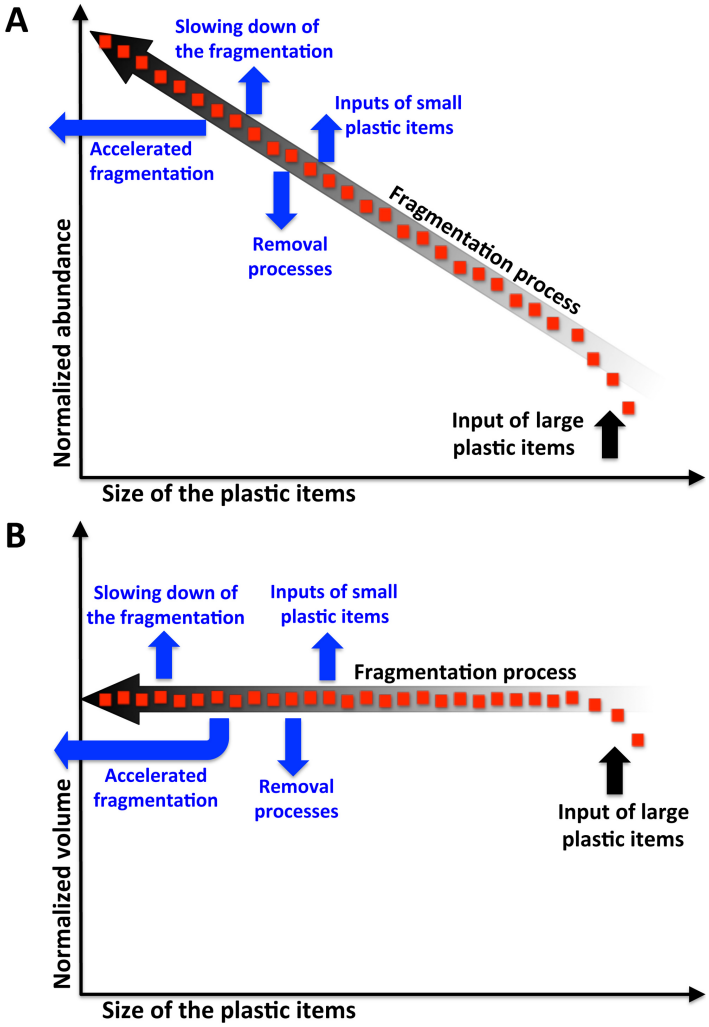

Fig. S9. Conceptual diagram of the main processes determining the shape of the size distribution of plastic in surface waters, in normalized abundance (A) and normalized volume (B). The power dependence of abundance on size can be linearized on a double log plot (red dots in A). Likewise, the log-log distribution of normalized volume by size classes should remain steady (red dots in B). Several processes (in blue) may lead to deviations from the log-log linearity. Domes or upward shifts in the linear size distribution can be caused by slowing down of the fragmentation process or significant inputs of small plastic items (e.g. industrial resin pellets). Troughs and gaps in the size distribution can be related to the acceleration of the fragmentation process or the occurrence of significant removal of plastic fragments (e.g. ingestion). Our study focus on an important trough in the plastic size spectrum (from few mm to microns), but cases of higher abundances toward small particles can be found in coastal marine environments (waters (S12) and sediments (S13, S14)) and lakes (S15). These small particles may be derived from fragmentation at sea but also from terrestrial inputs (e.g. textile fibers, microbeads used in cosmetic products), as suggested by some of these authors (S15). Indeed, textile fibers and microbeads are common in near shore environments, while they were negligible in our open-ocean sampling. Fragments, or broken pieces of larger objects, composed the majority of plastic items collected in the Malaspina Circumnavigation, in agreement with other samplings crossing plastic accumulation zones in the open ocean (S1, S16).

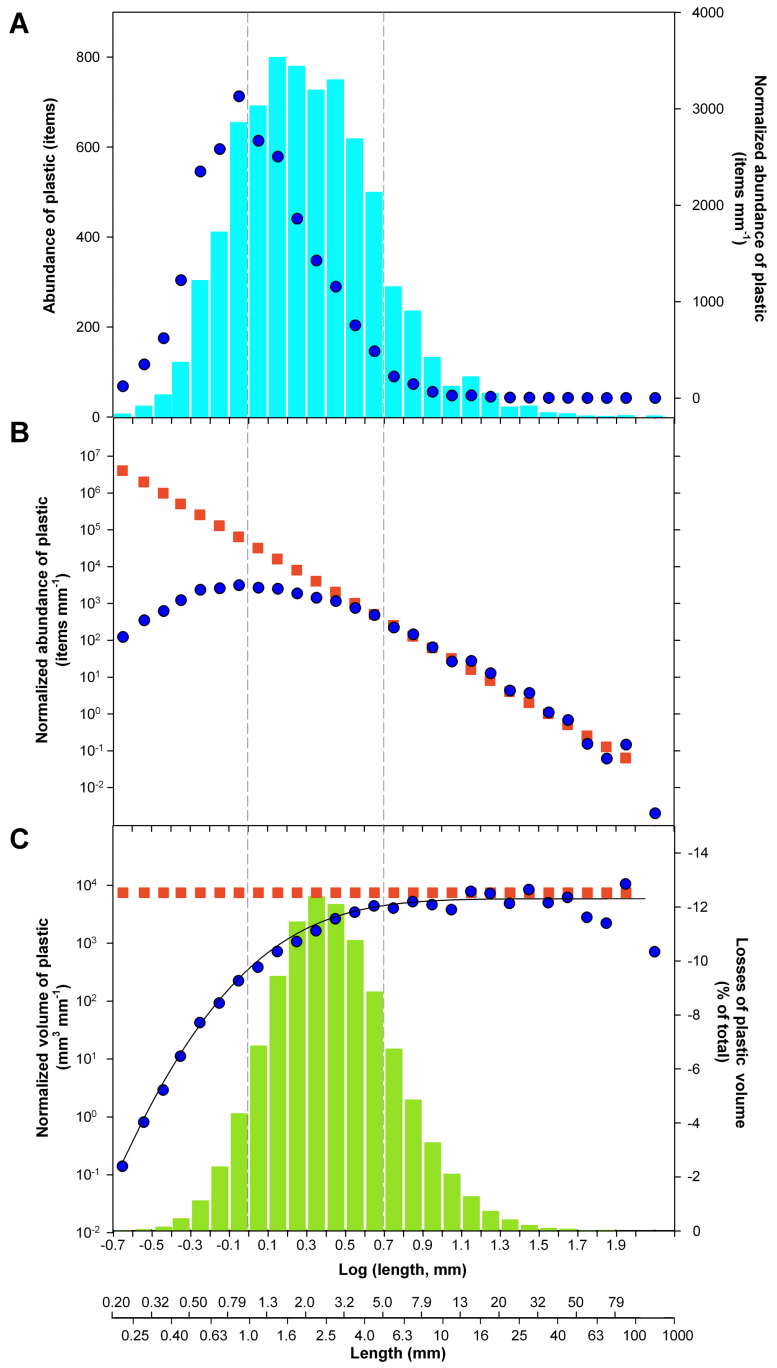

Fig. S10. Size distribution of plastic debris built with the material collected in all surface net tows in the Malaspina Circumnavigation (7359 items). (*A*) Size distribution in abundance (light blue bars) and normalized abundance (blue circles). (*B*) Measured (blue circles) and modeled (red squares) size distributions of normalized abundance of plastic in logarithmic scale. (*C*) Measured (blue circles) and modeled (red squares) size distributions of plastic in normalized volume. Green bars indicate the estimated losses of plastic volume by size class (Δ_i). Black line shows the measured size distribution after smoothing with a Weibull function (black line, $R = 0.9921$, $p < 0.0001$).

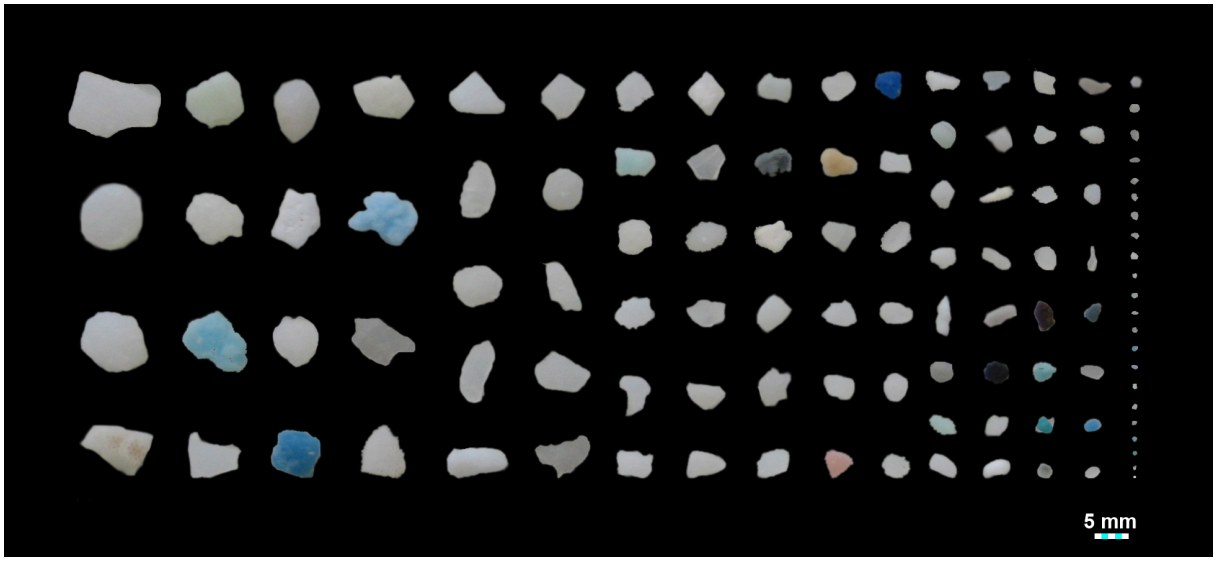

Fig. S11. Plastic fragments sampled on the ocean surface. This photography corresponds to the plastic items collected in a net tow in the South Atlantic Gyre.

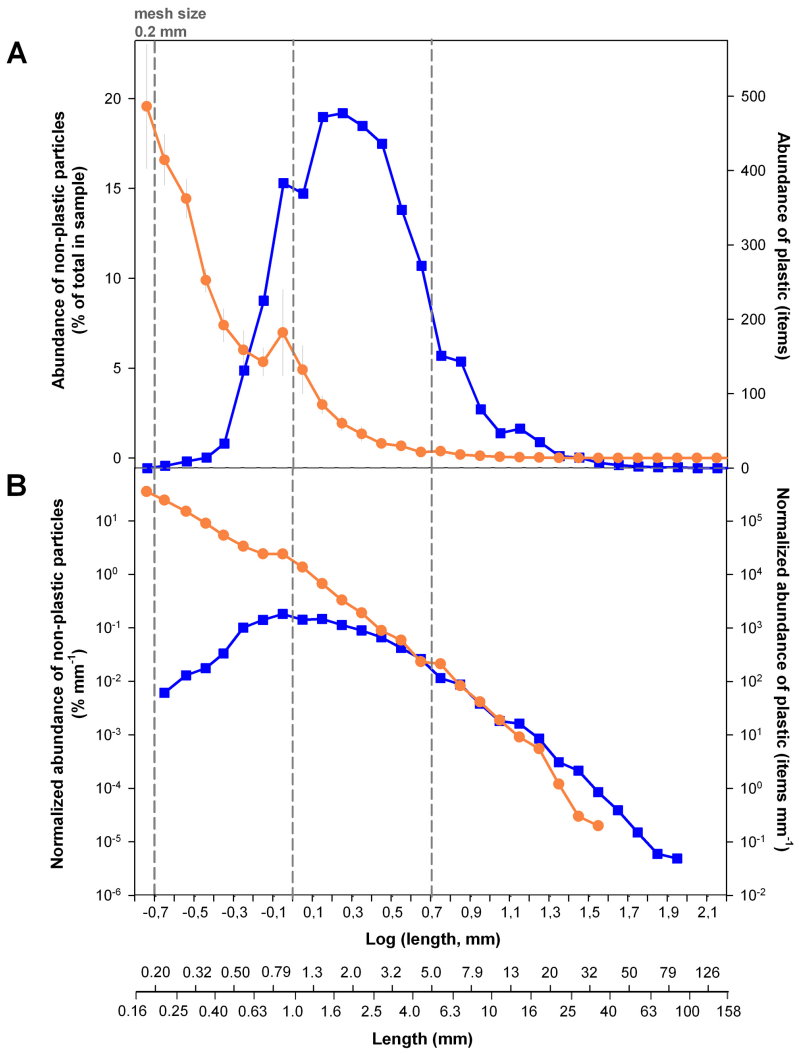

Fig. S12. Size distribution of non-plastic particles at six sites evenly distributed along the Malaspina circumnavigation (see Fig. S1 for location). (A) Size distribution in abundance. Orange line shows the averaged size distribution of non-plastic particles, computed as percentage of total in each sample to avoid over-representing the weight of samples with higher plankton abundance (left axis). Blue line shows the size distribution of plastic particles (right axis). (B) Size distribution in abundance normalized by the width (in mm) of the size class. Non-plastic particles are shown with orange line and plastic debris with blue line. The size distribution of non-plastic particles followed the expected power shape, with increasing abundances towards smaller sizes. The surface net used a 0.2-mm mesh, although it also collected abundant non-plastic particles in the 0.16-0.20 mm class likely due to mesh clogging. Vertical dashed lines show the thresholds of 0.2, 1.0 and 5.0 mm.

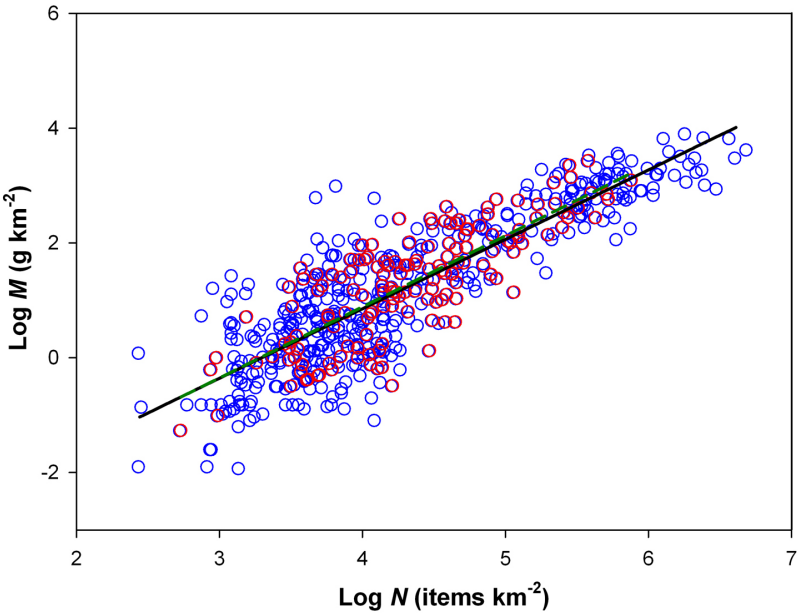

Fig. S13. Relationship between mass (*M*) and numerical (*N*) concentrations of plastic debris measured in the present study (n = 166, red open circles) and data from the literature (n = 404, blue open circles; refs. S2, S3, S17). Black line shows the log-log linear-square fitting on the whole dataset (log *M* (g km^{-2}) = 1.21· log *N* (items km^{-2}) - 3.99; n = 570, r = 0.8538, $p < 0.0001$). Green dashed line shows the log-log linear-square fitting on own data. Results suggest that the average size of plastic debris measured in Malaspina Circumnavigation is similar to that found for other world regions.

Supplementary References

S1. Law KL, et al. (2010) Plastic Accumulation in the North Atlantic Subtropical Gyre. *Science* 329:1185-1188.

S2. Doyle MJ, Watson W, Bowlin NM, Sheavly SB (2011) Plastic particles in coastal pelagic ecosystems of the Northeast Pacific ocean. *Mar Environ Res* 71:41-52.

S3. Goldstein MC, Rosenberg M, Cheng L (2012) Increased oceanic microplastic debris enhances oviposition in an endemic pelagic insect. *Biol Lett* doi: 10.1098/rsbl.2012.0298.

S4. Eriksen M, et al. (2013) Plastic pollution in South Pacific Subtropical Gyre. *Mar Pollut Bull* 15: 71-76.

S5. Reisser J, et al. (2013). Marine plastic pollution in waters around Australia: characteristics, concentrations, and pathways. *PLoS ONE* 8(11): e80466. doi:10.1371/journal.pone.0080466.

S6. Law KL, et al. (2014) Distribution of surface plastic debris in the eastern Pacific Ocean from an 11-year dataset. *Environ Sci Technol* 48:4732-4728.

S7. Kukulka T, Proskurowski G, Morét-Ferguson S, Meyer DW, Law KL (2012) The effect of wind mixing on the vertical distribution of buoyant plastic debris. *Geophys Res Lett* 39: L07601, doi: 10.1029/2012GL051116.

S8. Wang LP, Maxey MR (1993) Settling velocity and concentration distribution of heavy particles in homogeneous, isotropic turbulence. *J Fluid Mech* 256:27–68.

S9. Ruiz J, Macías D, Peters F (2004) Turbulence increases the average settling velocity of phytoplankton cells. *PNAS* 101: 17720–17724.

S10. Jiménez, J (1997) Oceanic turbulence at millimeter scales. *Sci Mar* 61(1): 47–56.

S11. Yakimets I, Lai D, Guigon M (2004) Effect of photooxidation cracks on behaviour of thick polypropylene samples. *Polym Degrad Stabil* 86:59–67.

S12. Cole M, et al. (2014) Isolation of microplastics in biota-rich seawater samples and organisms. Sci Rep 4:4528, doi: 10.1038/srep04528.

S13. Vianello A, et al. (2013) Microplastic particles in sediments of Lagoon of Venice, Italy: First observations on occurrence, spatial patterns and identification. *Estuar Coast Shelf Sci* 130:54-61.

S14. Browne, MA, Galloway TS, Thompson R.C. (2010). Spatial patterns of plastic debris along estuarine shorelines. *Environ Sci Technol* 44, 3404e3409.

S15. Eriksen M, et al. (2013a) Microplastic pollution in the surface waters of the Laurentian Great Lakes. *Mar Pollut Bull* 77:177-182.

S16. Morét-Ferguson S, et al. (2010) The size, mass, and composition of plastic debris in the western North Atlantic Ocean. *Mar Poll Bull* 60:1873-1878.

S17. Gilfillan LR, Ohman MD, Doyle MJ, Watson W (2009) Occurrence of plastic micro-debris in the southern California Current system. *Cal Coop Ocean Fish* 50:123–133.